Electronic Supplementary Information for:

Factors determining surface oxygen vacancy formation energy in ternary spinel structure oxides with zinc

Yoyo Hinuma[1,2*], Shinya Mine [3], Takashi Toyao[3,4], Takashi Kamachi[4,5], and Ken-ichi Shimizu[3,4]

[1] Department of Energy and Environment, National Institute of Advanced Industrial Science and Technology (AIST), 1-8-31, Midorigaoka, Ikeda 563-8577, Japan

[2] Center for Frontier Science, Chiba University, 1-33 Yayoicho, Inage, Chiba 263-8522, Japan

[3] Institute for Catalysis, Hokkaido University, N-21, W-10, Kita, Sapporo, Hokkaido 001-0021, Japan

[4] Elements Strategy Initiative for Catalysts and Batteries, Kyoto University, Katsura, Nishigyo, Kyoto 615-8520, Japan

[5] Department of Life, Environment and Materials Science, Fukuoka Institute of Technology, 3-30-1Wajiro-Higashi, Higashi-ku, Fukuoka 811-0295, Japan

* y.hinuma@aist.go.jp

Table SI-1. Geometry information on slab-and-vacuum models used in this paper.

Surface (cubic)	Compound	$\lvert\mathbf{a}'\times\mathbf{b}'\rvert$ (Å^2)	h_{cell} (Å)		h_{slab} (Å)		Atom count	
			Thin	Thick	Thin	Thick	Thin	Thick
(100)	$ZnAl_2O_4$	64.8	28.2	28.2	14.1	16.1	98	112
	$ZnGa_2O_4$	69.4	29.2	29.2	14.6	16.7	98	112
	$ZnIn_2O_4$	79.9	31.3	31.3	15.6	17.9	98	112
	ZnV_2O_4	70.8	29.4	29.4	14.7	16.8	98	112
	$ZnCr_2O_4$	68.7	29.1	33.3	14.6	18.7	98	126
	$ZnMn_2O_4$	68.6	29.9	29.9	15.0	17.1	98	112
	$ZnFe_2O_4$	69.9	29.2	29.2	14.6	16.7	98	112
	$ZnCo_2O_4$	63.8	28.0	31.9	14.0	16.0	98	112
(110)	$ZnAl_2O_4$	91.6	28.5	31.3	14.2	17.1	140	168
	$ZnGa_2O_4$	98.1	29.4	32.4	14.7	17.7	140	168
	$ZnIn_2O_4$	112.9	28.4	31.6	15.8	19.0	140	168
	ZnV_2O_4	100.2	29.7	32.6	14.8	17.8	140	168
	$ZnCr_2O_4$	97.2	29.4	32.4	14.7	17.7	140	168
	$ZnFe_2O_4$	98.9	29.5	32.4	14.7	17.7	140	168
	$ZnCo_2O_4$	90.2	28.2	31.1	14.1	16.9	140	168
(111)	$ZnAl_2O_4$	56.1	32.5	37.2	18.6	23.2	112	140
	$ZnGa_2O_4$	60.1	33.7	38.5	19.2	24.0	112	140
	$ZnIn_2O_4$	69.2	36.1	41.3	20.6	25.8	112	140
	ZnV_2O_4	61.2	34.0	38.8	19.4	24.3	112	140
	$ZnCr_2O_4$	59.7	33.6	38.3	19.2	24.0	112	140
	$ZnMn_2O_4$	60.7	33.8	38.6	19.3	24.1	112	140
	$ZnFe_2O_4$	60.5	33.8	38.6	19.3	24.1	112	140
	$ZnCo_2O_4$	55.2	32.3	36.9	18.4	23.1	112	140

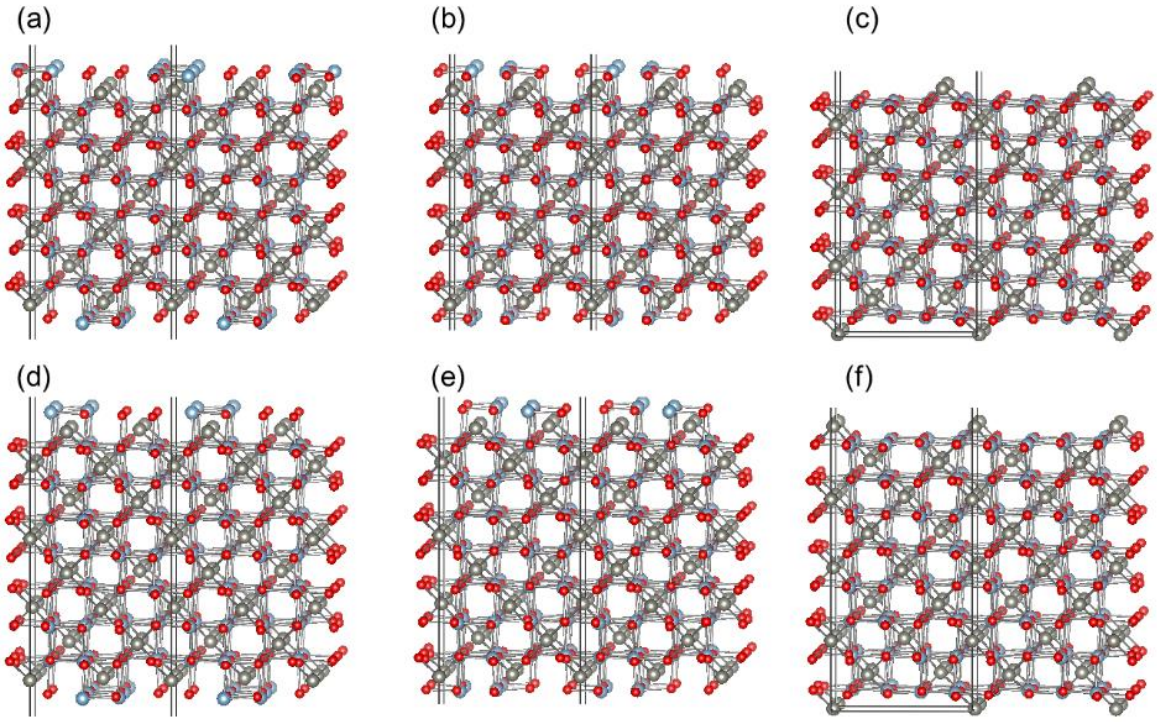

Fig. SI-1. Examples of $ZnAl_2O_4$ (100) surface slabs generated using Ref. 46 of the main text. The definition of transformation matrices and principal isometry follows Ref. 46. Lattice parameters indicate that the slab is a potential *tp* and thus $\boldsymbol{T}_1 = \boldsymbol{I}$. The top layer is either the Al-O layer or the Zn layer. $\boldsymbol{T}_2 = \boldsymbol{T}_{45\mathrm{deg}}$ in all examples, and the principal isometry is 2_y in Figs. 3a,b,f and $\bar{1}$ in Fig. 3c-e. The total number of severed bonds per surface of the (100) *n*-double cell is four from Zn, six from Al, and 10 from O in Figs. SI-1(a,b,d,e) and two, four, and six in Figs. SI-1(c,f), respectively. Therefore, the termination in Figs. SI-1(c,f) is expected to be much stable than those in Figs. SI-1(a,b,d,e). Interestingly, the same termination can be obtained with a different principal isometry when the slab thickness is varied. The termination in Figs. SI-1(c,f) can be made more stable by manually tilting the two-fold coordinated Zn at the surface toward the slab such that these Zn are closer to more O, and this procedure was actually performed in this study.

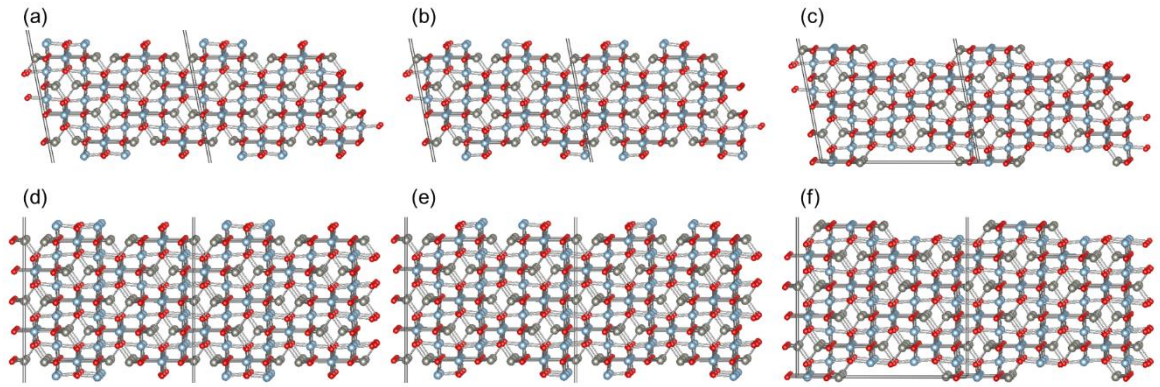

Fig. SI-2. Examples of $ZnAl_2O_4$ (110) surface slabs generated using Ref. 46 of the main text. The definition of transformation matrices and principal isometry follows Ref. 46. Lattice parameters indicate that the slab is not *hp*, *tp*, nor *oc* and $\boldsymbol{T}_1 = \boldsymbol{I}$. The top layer is either the Al-Zn layer or the Al-Zn-O layer. $\boldsymbol{T}_2 = \boldsymbol{T}_{12}$ in all examples, and the principal isometry is 2_y penetrating $\bar{1}$ in Figs. SI-2(a,b,f) and 2_{1y} penetrating $\bar{1}$ in Figs. SI-2(c-e). The total number of severed bonds per surface of the (110) *n*-double cell is four from Zn, six from Al, and 10 from O in Figs.SI-2(a,b,d,e) and four, eight, and 10 in Figs.SI-2(c,f), respectively. The termination in Figs.SI-2(c,f) is expected to be slightly unstable but calculations on $ZnAl_2O_4$, $ZnGa_2O_4$, and $ZnIn_2O_4$ show that this termination is clearly more stable than those in Figs.SI-2(a,b,d,e).

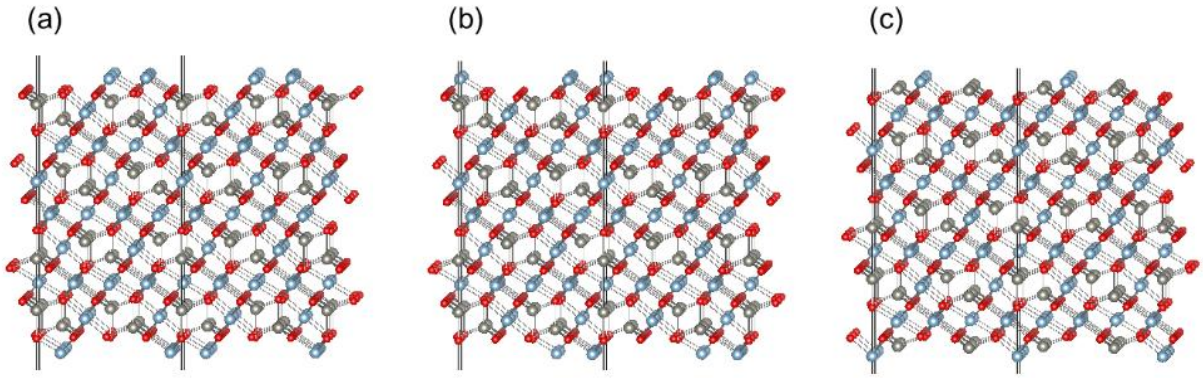

Fig. SI-3. Examples of $ZnAl_2O_4$ (111) surface slabs generated using Ref. 46 of the main text. The definition of transformation matrices and principal isometry follows Ref. 46. Lattice parameters indicate that the slab is a potential *hp* and $\boldsymbol{T}_1$ is determined accordingly. The top layer is either the Al-Zn layer but the second layer can be either O or Zn. $\boldsymbol{T}_2 = \boldsymbol{I}$ and the principal isometry is 2_y penetrating $\bar{1}$ in all cases. There are two and one choices of x_c in the former (Fig. SI-3(a-b)) and latter (Fig. SI-3(c)) cases, respectively. The total number of severed bonds per surface of the (111) *n*-double cell is zero from Zn, nine from Al, and nine from O in Fig. SI-3(a), zero, nine, and nine in Fig. SI-3(b), and two, three, and five in Fig. SI-3(c), respectively. Therefore, the termination in Fig. SI-3(c) is expected to be more stable than those in Fig. SI-3(a-b).

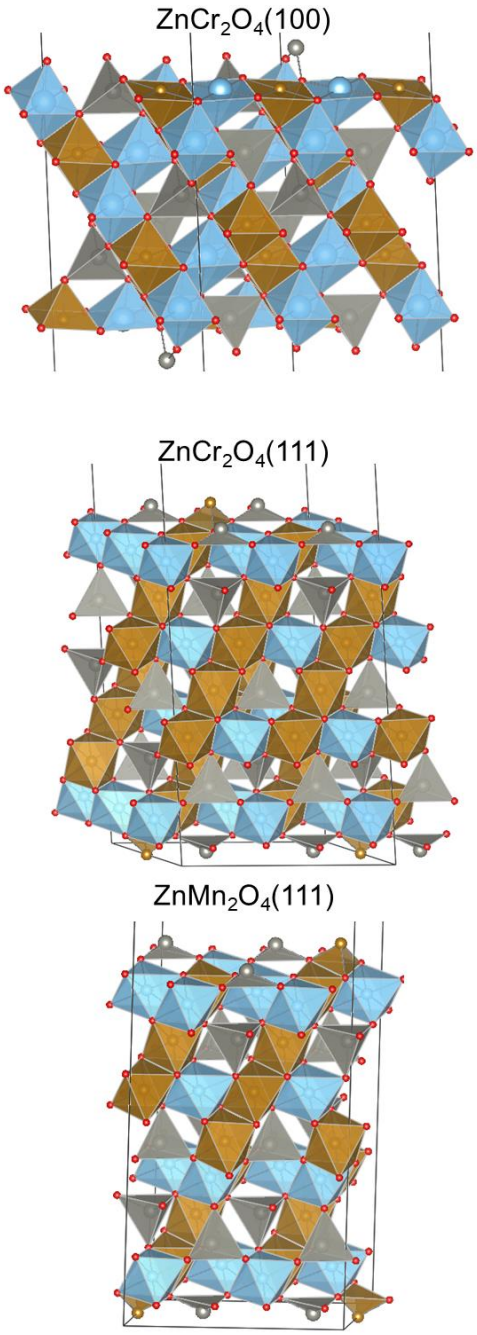

Fig. SI-4. Employed terminations of ZnM_2O_4 surfaces other than those shown in Fig. 1 of the main text. Gray, brown, blue, and red balls indicate Zn, spin-up M, spin-down M, and O.

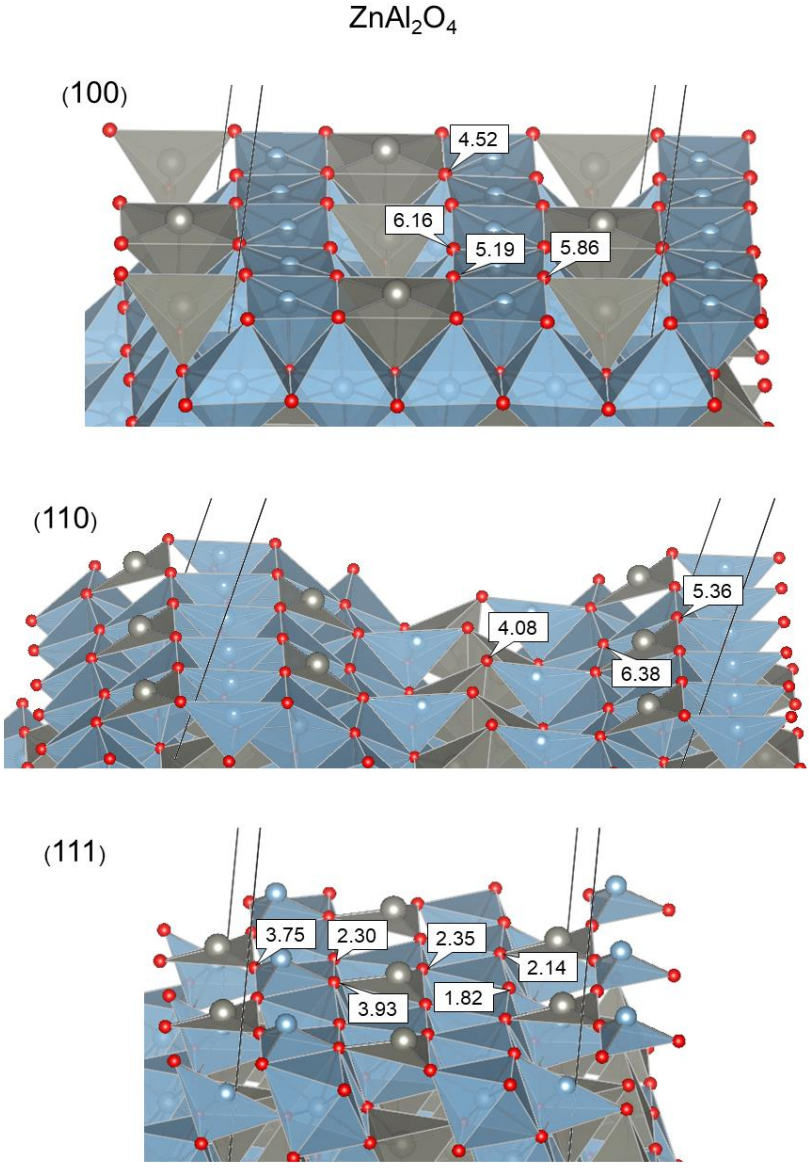

Fig. SI-5. E_{Ovac} in eV/defect for various O positions in $ZnAl_2O_4$. Gray, blue, and red balls indicate Zn, Al, and O, respectively.

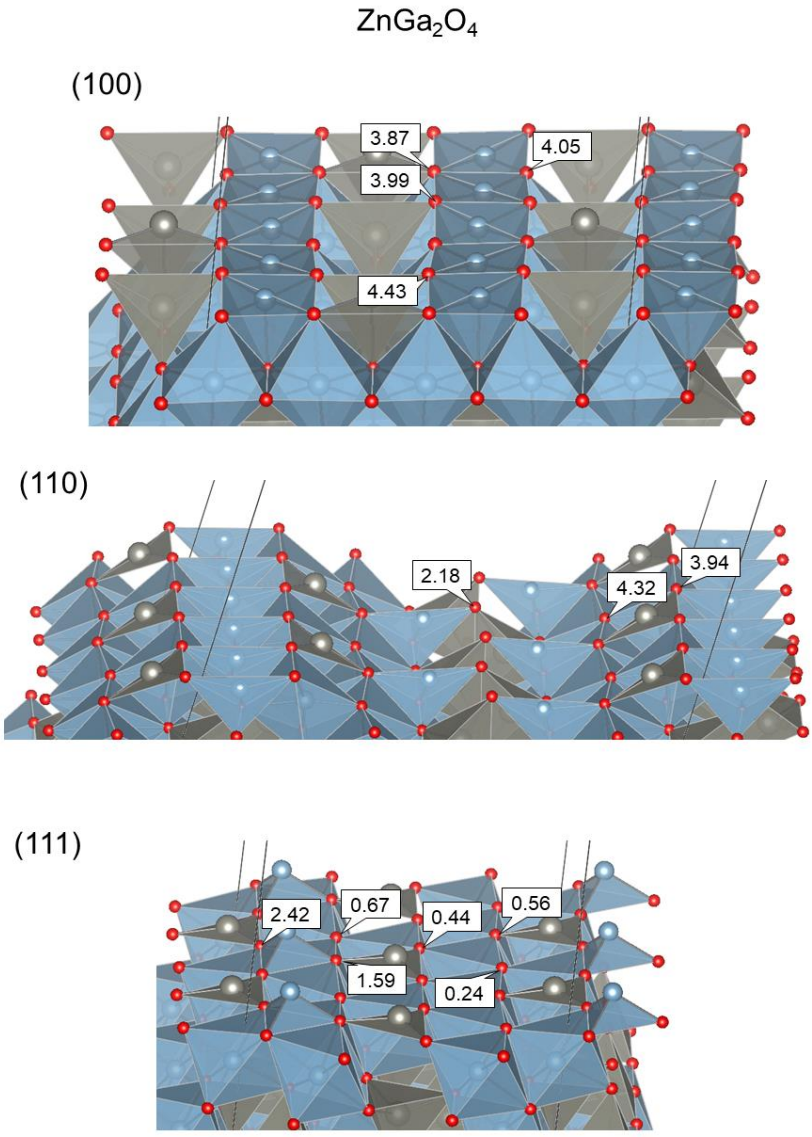

Fig. SI-6. E_{Ovac} in eV/defect for various O positions in $ZnGa_2O_4$. Gray, blue, and red balls indicate Zn, Ga, and O, respectively.

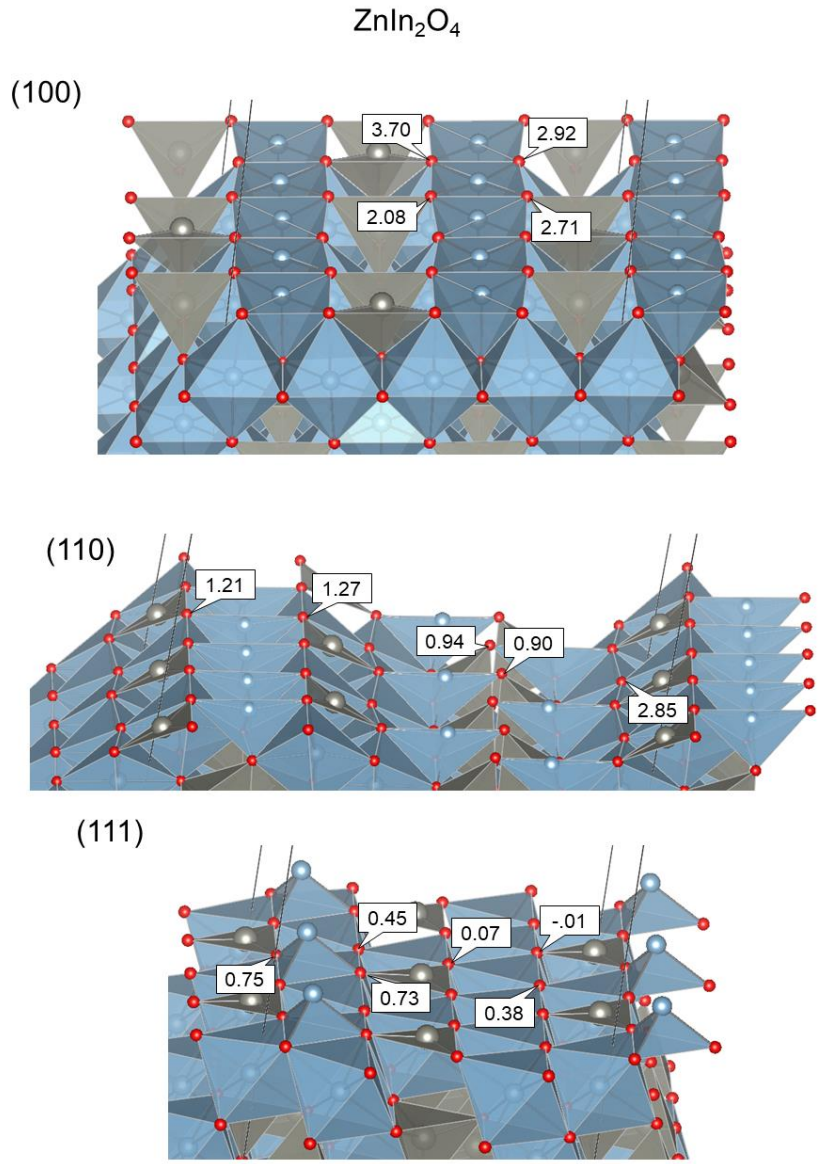

Fig. SI-7. E_{Ovac} in eV/defect for various O positions in $ZnIn_2O_4$. Gray, blue, and red balls indicate Zn, In, and O, respectively.

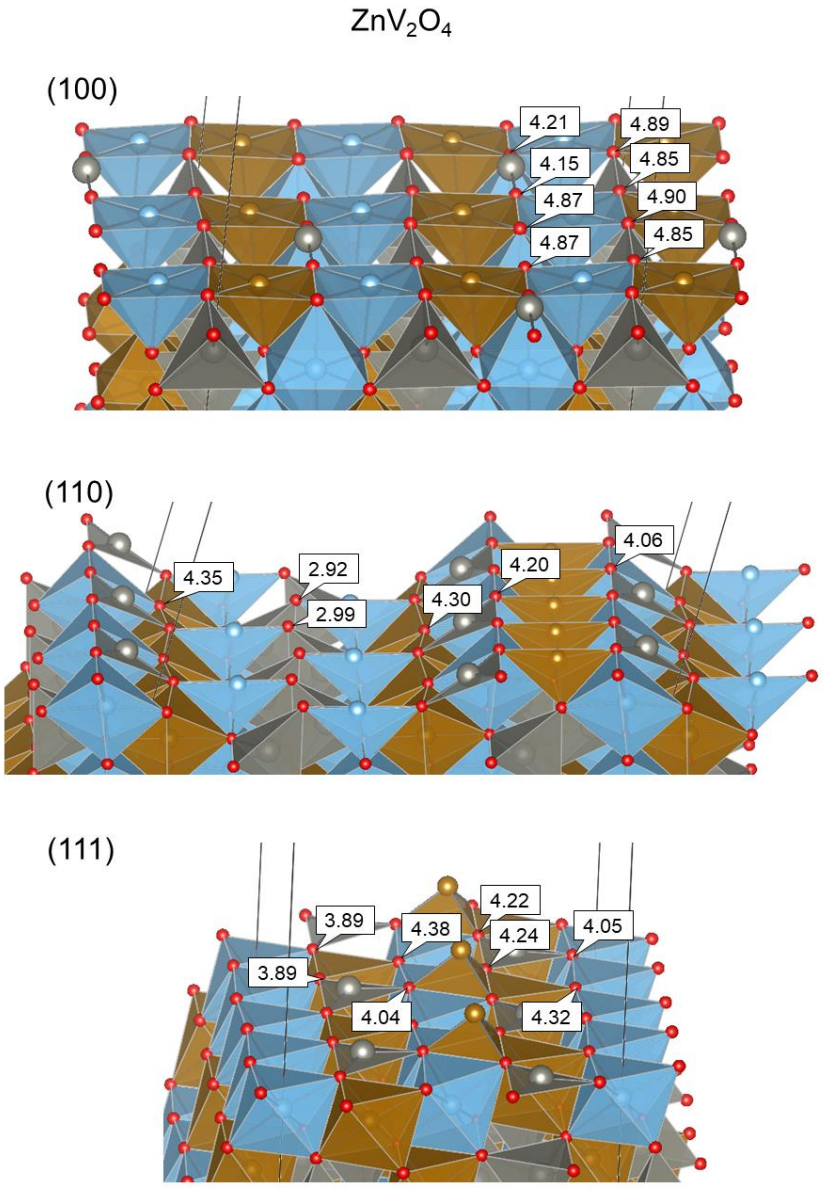

Fig. SI-8. E_{Ovac} in eV/defect for various O positions in ZnV_2O_4. Gray, brown, blue, and red balls indicate Zn, V (spin-up), V (spin-down), and O, respectively. The spin for V is that when cleaved from bulk.

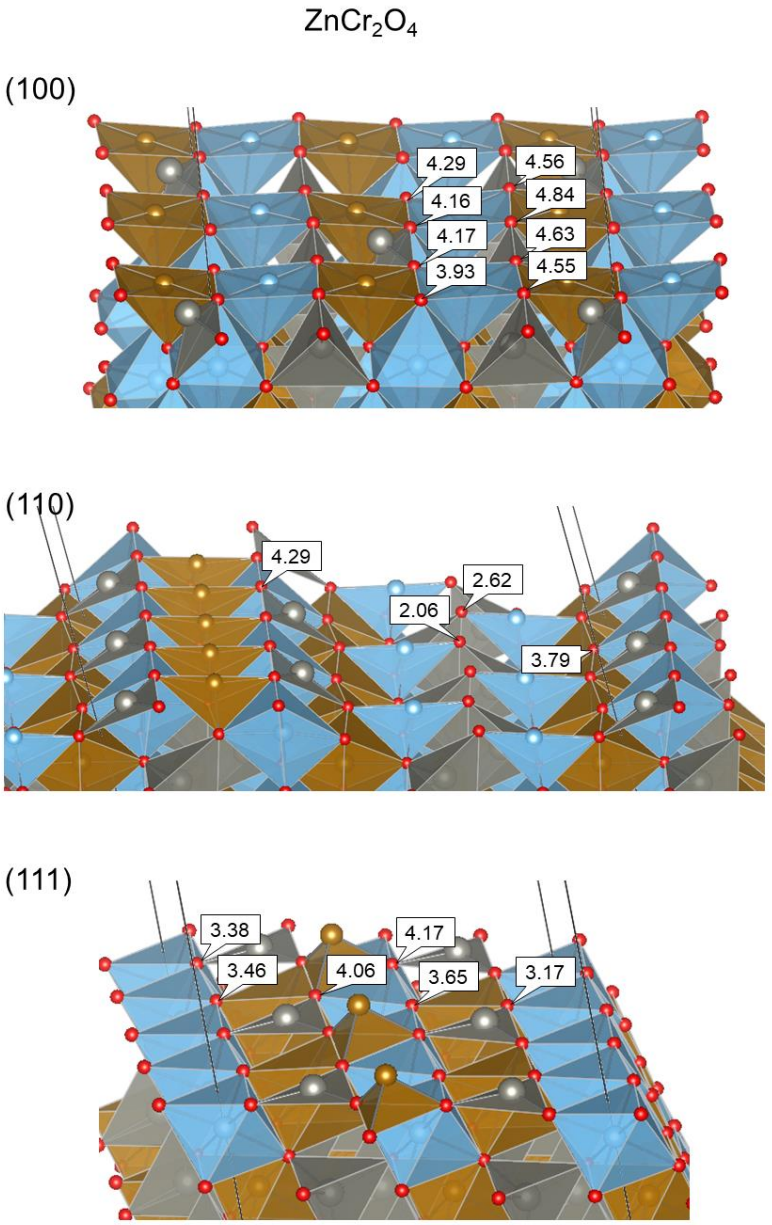

Fig. SI-9. E_{Ovac} in eV/defect for various O positions in $ZnCr_2O_4$. Gray, brown, blue, and red balls indicate Zn, Cr (spin-up), Cr (spin-down), and O, respectively. The spin for Cr is that when cleaved from bulk.

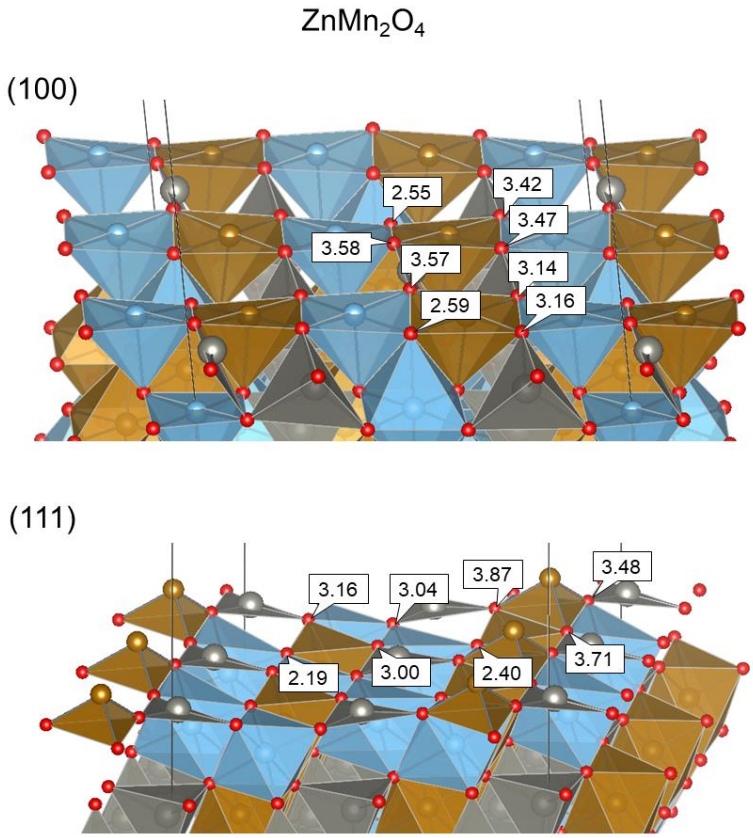

Fig. SI-10. E_{Ovac} in eV/defect for various O positions in $ZnMn_2O_4$. Gray, brown, blue, and red balls indicate Zn, Mn (spin-up), Mn (spin-down), and O, respectively. The spin for Mn is that when cleaved from bulk.

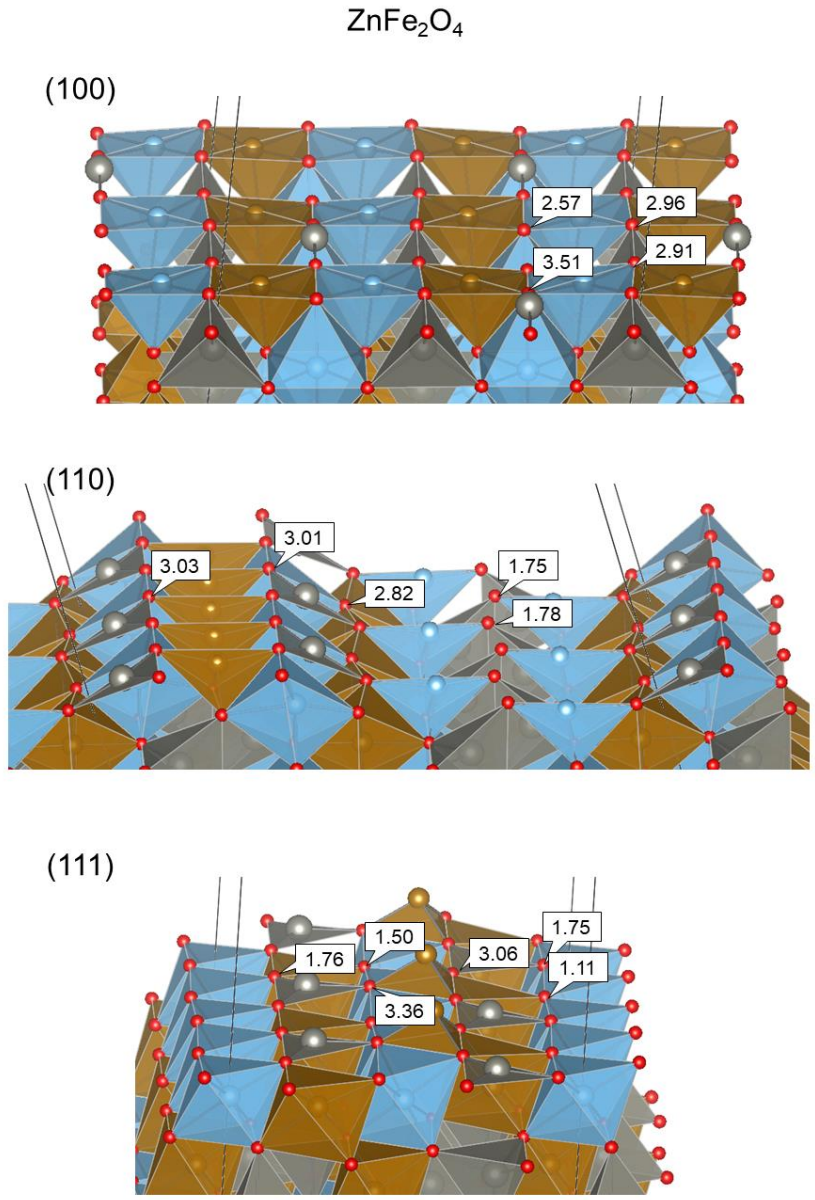

Fig. SI-11. E_{Ovac} in eV/defect for various O positions in $ZnFe_2O_4$. Gray, brown, blue, and red balls indicate Zn, Fe (spin-up), Fe (spin-down), and O, respectively. The spin for Fe is that when cleaved from bulk.

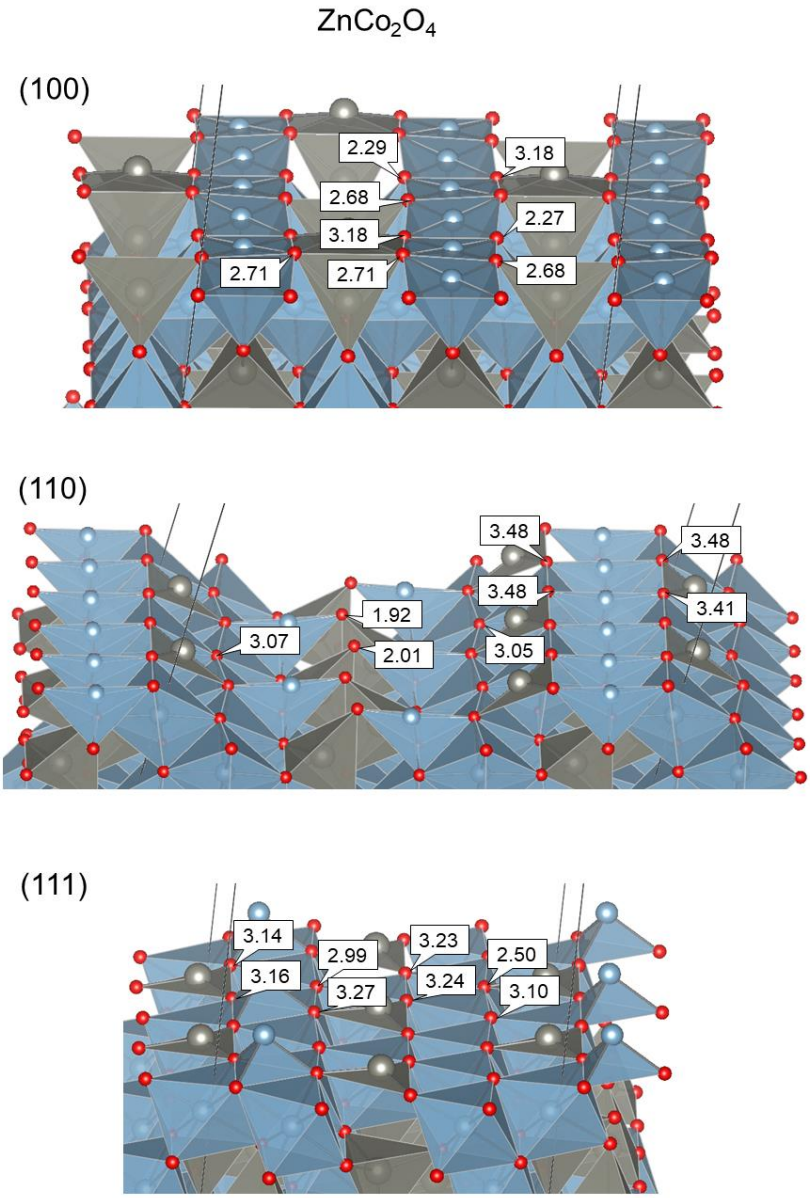

Fig. SI-12. E_{Ovac} in eV/defect for various O positions in $ZnCo_2O_4$. Gray, blue, and red balls indicate Zn, Co, and O, respectively.

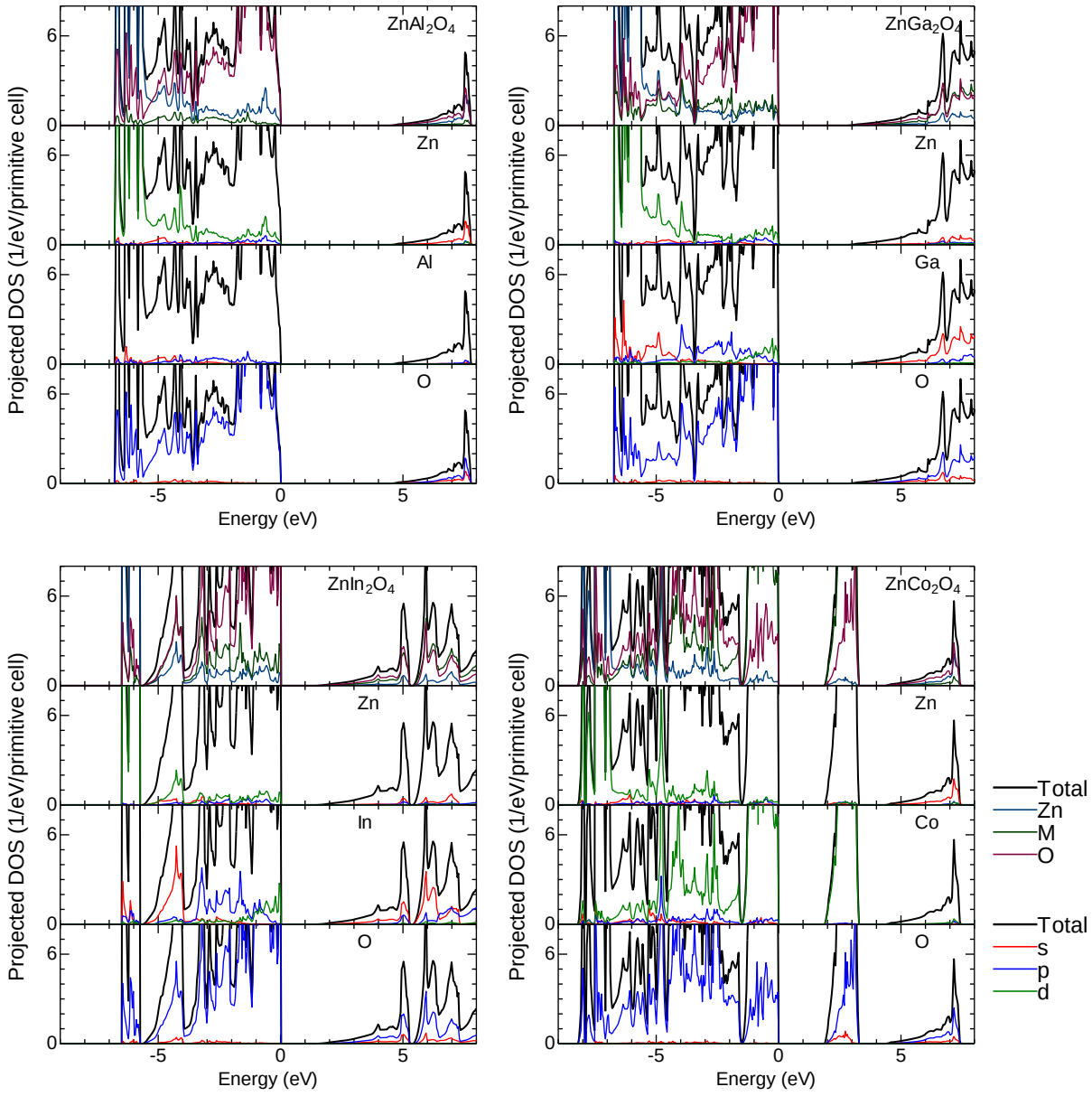

Fig. SI-13. Site-projected DOS of ZnM_2O_4. The sums of projected DOS by species and by orbital character are shown. The primitive cell contains two Zn, four M, and eight O atoms.

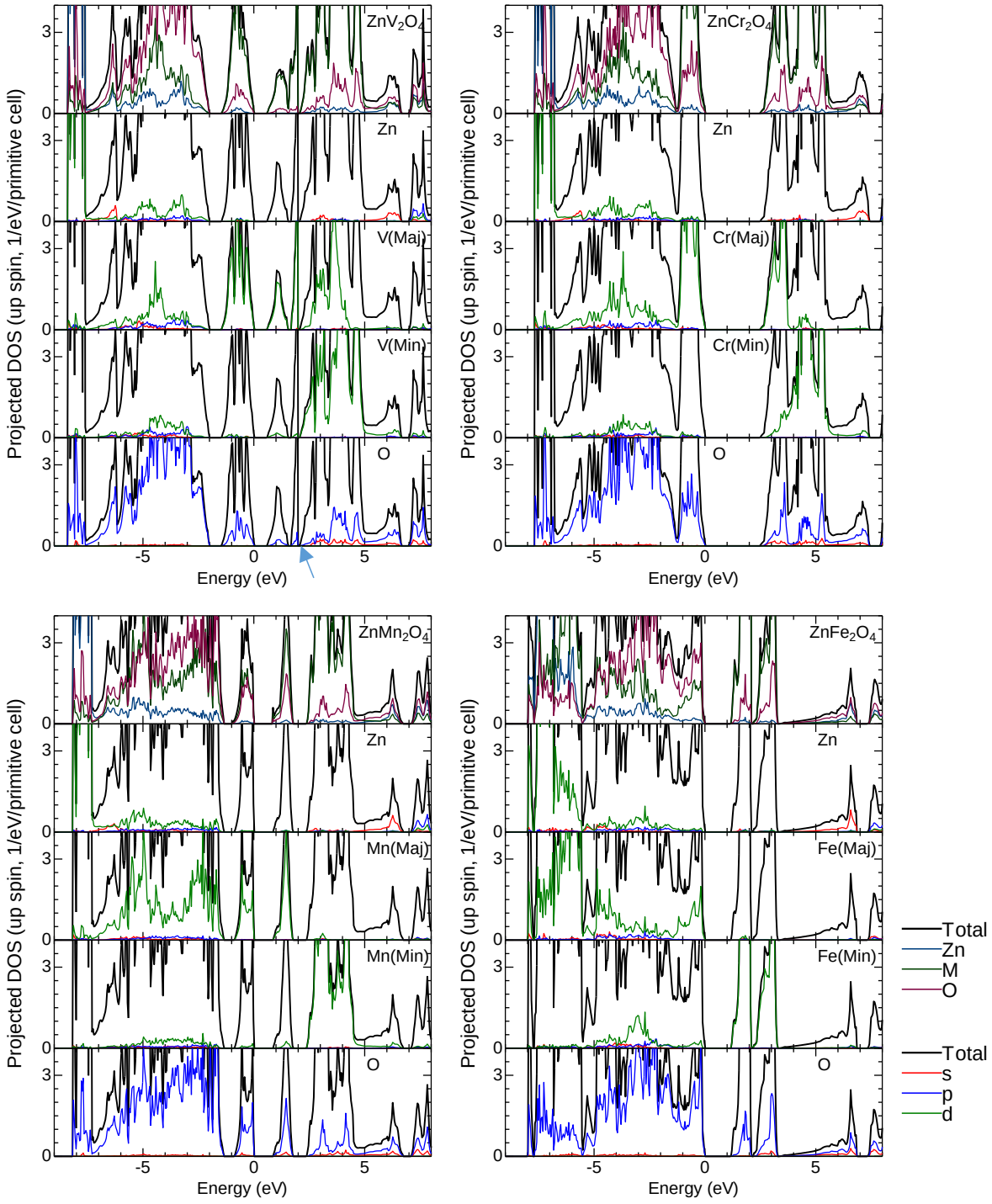

Fig. SI-14. Site-projected DOS of ZnM_2O_4. The sums of projected DOS by species and by orbital character are shown. The primitive cell contains two Zn, four M, and eight O atoms. For these spin polarized systems, only the spin up DOS is shown for Zn and O and the spin up DOS are drawn separately as M(Maj) and M(Min) for the two pairs of M atoms where spin up is the majority and minority spin, respectively. The arrow in ZnV_2O_4 indicates the bottom of the V minority 3*d* (t_{2g}) band.

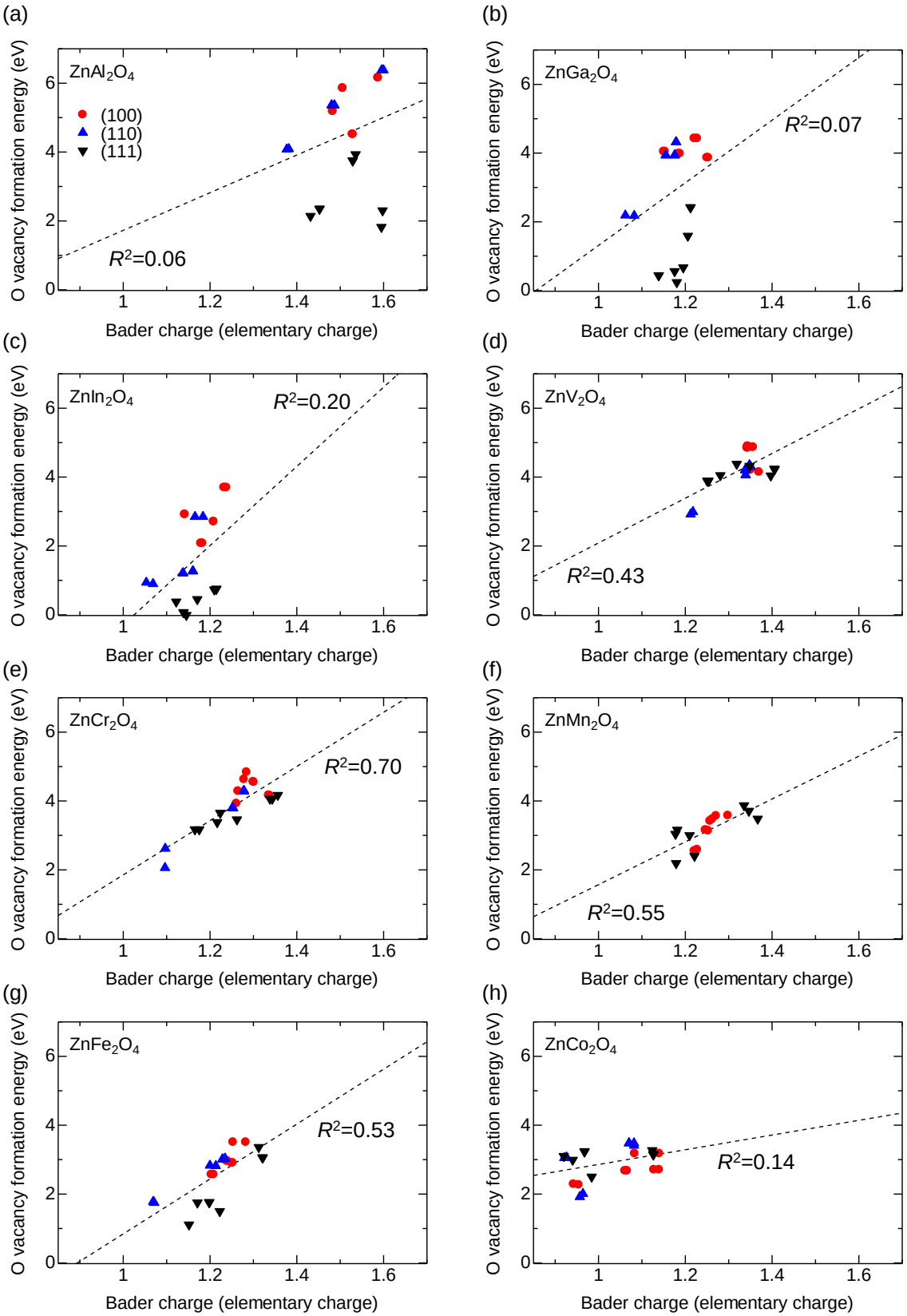

Fig. SI-15. Plots of E_{Ovac} versus the absolute value of the Bader charge at the desorbing O site for each ZnM_2O_4. Points are labeled by orientation, and the least-squares fit line is over all points.

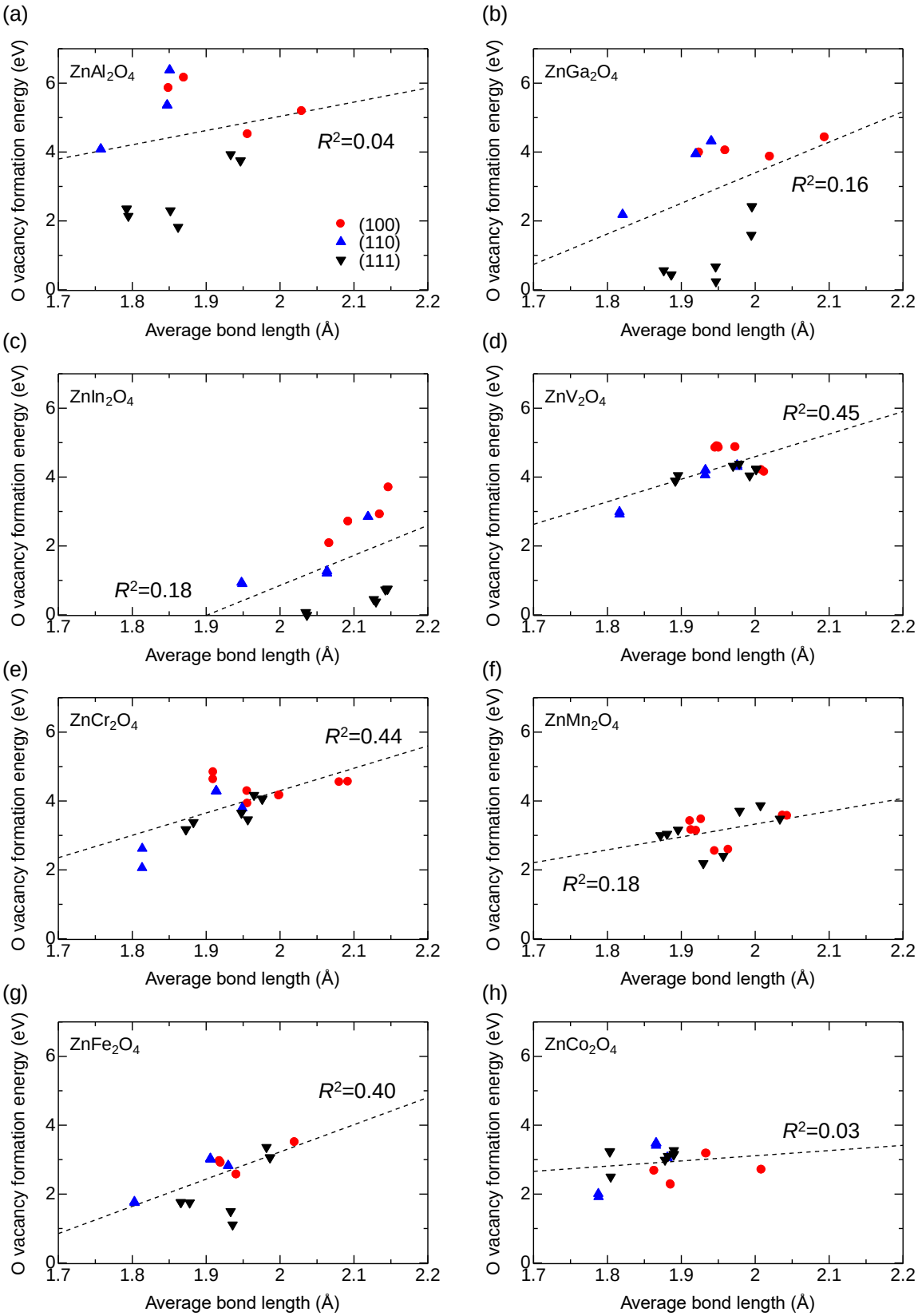

Fig. SI-16. Plots of E_{Ovac} versus average O-cation bond length at the desorbing O site for each ZnM_2O_4. Points are labeled by orientation, and the least-squares fit line is over all points.

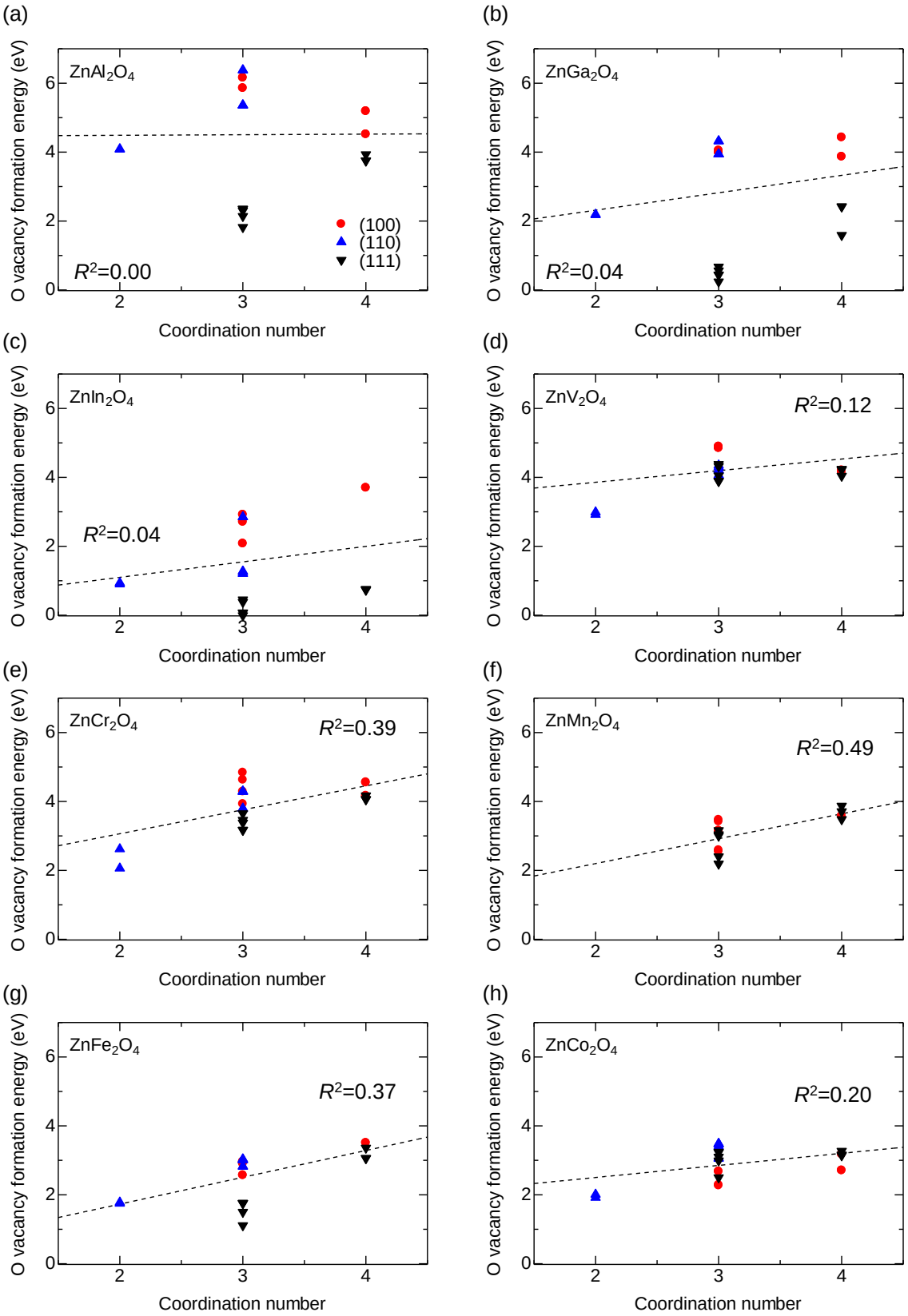

Fig. SI-17. Plots of E_{Ovac} versus coordination number at the desorbing O site for each ZnM_2O_4. Points are labeled by orientation, and the least-squares fit line is over all points.